Node-Diamond approximation of heterogeneous and anisotropic diffusion systems on arbitrary two-dimensional grids

El-Houssaine Quenjel, Abdelaziz Beljadid

Node-Diamond approximation of heterogeneous and anisotropic diffusion systems on arbitrary two-dimensional grids

El Houssaine QUENJEL[1,*] and Abdelaziz BELJADID[2,3]

[1]Chair of Biotechnology, LGPM, CentraleSupélec, CEBB, 3 rue des Rouges Terres, 51110 Pomacle, France, el-houssaine.quenjel@centralesupelec.fr

[2]International Water Research Institute, Mohammed VI Polytechnic University, Green City, 43150, Morocco

[3]Department of Mathematics and Statistics, University of Ottawa, Ottawa, ON, K1N 6N5, Canada, abeljadi@uottawa.ca

August 13, 2021

Abstract

We develop a new nodal numerical scheme for solving diffusion equations. Anisotropic and heterogeneous diffusion tensors are taken into account in these equations. The method allows to cover a wide range of general meshes such as non-confirming and distorted ones. The main idea consists in deriving the scheme from a discrete bilinear form using cellwise approximation of the diffusion tensor and particular discrete gradients. These gradients are conceived on diamonds partitioning the cell using local geometrical objects. The degrees of freedom are placed at the centers and vertices of cells. The cell unknowns can be eliminated without any fill-in. As a result, the coercivity of the scheme holds true unconditionally by construction. The convergence theorem of the Node-Diamond scheme is proved under classical assumptions on the physical parameters of the model equation and the mesh. Numerical results show the good behavior of the proposed approach on various examples among which we consider strongly anisotropic and heterogeneous systems. For instance, optimal accuracy consisting of quadratic rates for L^2-errors and linear rates for H^1-errors is obtained.

1 Introduction

We develop and analyze a novel numerical scheme approximating second-order elliptic problems with Dirichlet boundary conditions. In view of its wide practical applications, we focus on the following model

$$-\nabla \cdot \kappa(x)\nabla u = f \quad \text{in } \Omega, \tag{1.1}$$

$$u = g \quad \text{on } \partial\Omega, \tag{1.2}$$

where u is the main unknown and Ω is a bounded open connected domain of $\mathbb{R}^d$ ($d \geq 1$) with a Lipschitz boundary $\partial\Omega$. The matrix κ accounts for the anisotropic heterogeneous diffusion tensor. The right-hand side f models the source and sink terms. The boundary condition is prescribed by a given function g. Equation (1.1) stems from the conservation principle of a steady problem together with a constitutive law such as Fick's law if u represents the temperature or

Darcy's law if u denotes the hydraulic head. The diffusion term $-\nabla\cdot\kappa(x)\nabla u$ is a cornerstone term in many practical problems arsing in porous media flows, semiconductor models and systems of population dynamics.

The main hypotheses on the physical parameters of the model (1.1) are given as follows

$$\kappa \in L^\infty(\Omega)^{d\times d} \text{ is a symmetric uniformly coercive tensor i.e.}$$
$$\exists \underline{\kappa}, \overline{\kappa} > 0 \ : \underline{\kappa}\,|v|^2 \le \kappa(x)v\cdot v \le \overline{\kappa}\,|v|^2, \quad \forall \text{ a.e. } x\in\Omega,\ v\in\mathbb{R}^d, \tag{1.3a}$$
$$f \in L^2(\Omega), \quad g \in H^{1/2}(\partial\Omega). \tag{1.3b}$$

These assumptions allow to ensure the well-posedness of the problem (1.1)-(1.2) in the weak sense. Then, $u \in H^1(\Omega)$ is a weak solution if and only if its solves the variational formulation

$$\begin{cases} \displaystyle\int_\Omega \kappa(x)\nabla u\cdot\nabla\varphi\,\mathrm{d}x = \int_\Omega f\varphi\,\mathrm{d}x, & \forall\varphi\in H^1_0(\Omega), \\ \gamma(u) = g, & \text{in } H^{1/2}(\partial\Omega), \end{cases} \tag{1.4}$$

where γ is the trace operator defined from $H^1(\Omega)$ into $H^{1/2}(\partial\Omega)$. It is well-known that (1.1)-(1.2) has a unique weak solution in the aforementioned sense using the famous Lax-Milgram theorem.

The objective of this paper is to develop and validate a new nodal numerical scheme, with crucial theoretical and computational features, for approximating the weak solution of (1.4). A "good" numerical scheme should be consistent, convergent, optimally accurate, robust, yields a small stencil and satisfy the discrete maximum principle on generic meshes and diffusion tensors. The design of such scheme is very challenging. A large number of previous studies is conducted for the numerical resolution of (1.4). These studies deal with a single or a couple of the aforementioned proprieties. In the following, we briefly review some of them.

It is well known that finite elements [11] are suitable for elliptic problems on particular conforming meshes such as simplices. Advanced schemes of type finite volumes [15, 19, 28], Hybrid Mimetic Mixed (HMM) methods [13, 18] have greatly contributed in the discretization of diffusion operators, especially when rough data are prescribed and the mesh is quite general. More specifically, the TPFA (Two-Point Flux Approximation) scheme is the simplest finite volume method and possesses an elegant structure yielding a very parse stiffness matrix which is further an M-matrix. The simplicity is a result of a restrictive orthogonality condition on the mesh together with assuming a scalar tensor κ. The aim is to evaluate the flux only in the normal direction to the interface in a consistent way. Its foundation and analysis give deep insights on the construction and study of multi-point methods. For instance, we mention the MPFA (Multi-Point Flux Approximation) approach [1, 2, 3, 4] that extends some ideas of the TPFA scheme. The objective is to consistently approximate the fluxes using several directions mainly linking cell degrees of freedom (d.o.f) to account for anisotropy, discontinuity of the diffusion tensor and distortion of the mesh. On the other hand, the coercivity is tensor and mesh dependent and it may be lost in the case where the anisotropic ratio is important. This can lead to possible negative eigenvalues of the stiffness matrix entailing spurious oscillation on the solution and loss of convergence. Among schemes enabling consistency and coercivity, we first cite the DDFV (Discrete Duality Finite Volume) method [6, 14, 25, 26, 29]. The construction of approximate fluxes, and also the gradient on diamond subsets, involve cell and vertex unknowns which may increase the computational cost. A particular treatment is needed when κ is discontinuous across (primal and dual) interfaces since the gradient are not cellwise constants [7]. Next, the HMM schemes [10, 16, 20] are derived from a discrete weak formulation using cellwise gradients together with a stabilization term. They employ cell and edge unknowns and this increases the complexity of the resulting algorithm. To reduce the number of d.o.f, a small stencil nodal method referred to as the VAG (Vertex Approximate Gradient) scheme was introduced in [21]. The key idea is to interpolate the interface unknowns using its vertices. It is also possible to get rid of the stabilization term by considering P_1 finite element gradients on a simplicial sub-mesh [9, 8]. The VAG method is reformulated thanks to some "generalized" fluxes acting between

the cell and its surrounding vertices. In each cell, the local cell-vertex flux has to include the contributions of the other vertices, even if they are not connected, so that the coercivity can be maintained. An important feature of the VAG discretization consists in the ability to eliminate the cell unknowns due to a static condensation. A relative weakness is that the P_1 gradients are sometimes computed on a flattened sub-mesh even if the initial mesh presents good shape qualities. For instance, this is the case of initial triangular meshes with acute angles. Finally, we indicate that most of the aforementioned methods enter the abstract framework referred to as the gradient discretization method [17].

In this study, we propose a new nodal discretization that we will call the Node-Diamond scheme. Its derivation draws some inspirations from the HMM, VAG and DDFV methods. It is elaborated thanks to two key ingredients. First, as a starting point, we set and take advantage of the discrete bilinear form and the cellwise approximation of diffusion tensor. Second, we design local embedded diamonds using the cell, one vertex and the two edges sharing this vertex. The diamond region offers adequate geometrical objects to approximate the gradient in a consisting way. More importantly, edge unknowns are not mandatory and they are expressed in terms of their extreme vertices. We prove that the discrete Poincaré's inequality is fulfilled. Consequently, the scheme coercivity and the existence of the numerical solution hold unconditionally. Owing to ideas from the finite volumes literature, a natural extension to an additional convection term is highlighted without technical issues. By proving an asymptotic Stokes' formula, we demonstrate the convergence of the Node-Diamond scheme. In particular, the sequence of numerical solutions converges to the unique solution of (1.4) in the sense of H^1-norm. As in the context of the VAG methodology, the cell unknowns, used in the Node-Diamond scheme, can be eliminated without any fill-in. In other words, only nodal unknowns are involved in the resolution process after computing a simple Schur complement. Contrary to the VAG scheme, the Node-Diamond cell-vertex flux takes into account only connected d.o.f to the vertex in question. Moreover, there is no need to simplicial sub-mesh nor the stabilization. Also, advective fluxes can be computed in a straightforward way across interfaces of control volumes made of halves of diamond cells. Finally, we below summarize the central strengths of the Node-Diamond scheme.

- Highly heterogeneous and strongly anisotropic tensors can be taken into account.
- The scheme enables the use of quite general polygonal meshes (non-conforming, non-structured, distorted, ...).
- Coercivity is guaranteed unconditionally.
- Nodal unknowns are only involved after the elimination of the cell ones without any fill-in.
- A compact stencil of 9 points on quadrangular meshes is generated, which ensures the sparsity of the stiffness matrix.
- The method is robust and second order accurate.

The rest of the paper is outlined as follows. Section 2 is devoted to the establishment of the discrete setting. Precisely, local description of the involved d.o.f are specified using the cell-vertex connectivity. Embedded diamonds are then constructed and they provide appropriate objects to uniquely design a whole consistent and accurate approximation of the gradient operator. A discrete counterpart of Poincaré's inequality is stated and proved. Section 3 focuses on the derivation and the numerical analysis of the Node-Diamond scheme. Then, the coercivity of the scheme is proved and the convergence theorem is shown. A particular emphasis is placed on the identification of the limit, which is not obvious. Finally, Section 4 presents numerical results. They are preceded by some guidelines on the implementation. Several typical problem-cases of the literature are tested, where quite general meshes, strongly anisotropic and heterogeneous tensors are taken into account. They exhibit the robustness and accuracy of the Node-Diamond scheme and its capability to deal with the heterogeneity of the system and geometries of meshes.

2 Mesh, discrete spaces and operators

In this section, we define the domain discretization, specify the approximate spaces, where discrete variables live, and show the construction the approached gradient operator. We will focus on systems of two dimensions.

2.1 Domain discretization

Let us first introduce the main objects and notations that are mandatory to construct the Node-Diamond numerical scheme. Let $\mathcal{T}$ be a decomposition of Ω into non-overlapping connected subsets C such that $\bigcup_{C\in\mathcal{T}} \overline{C} = \overline{\Omega}$, where the topological interior of any cell $C \in \mathcal{T}$ is not the empty set. It is also supposed that C is star-shaped with respect to its mass center denoted by x_C. We assume that each edge of the mesh is shared by at most two cells. Let $\mathcal{S}_C$ be the set generating the C-cell vertices. The set of the mesh vertices is given by $\mathcal{S} = \bigcup_{C\in\mathcal{T}} \mathcal{S}_C$. The position of each vertex $\mathbf{v} \in \mathcal{S}_C$ is denoted by $x_\mathbf{v}$. The family $\mathcal{T}_\mathbf{v}$ refers to the cells sharing the vertex $\mathbf{v}$. The set of boundary (Dirichlet) vertices is denoted by $\mathcal{S}^D$. We consider $d_{C,\mathbf{v}} = \mathbf{dist}(C, \mathbf{v})$, where $\mathbf{dist}$ stands for the Euclidean distance on $\mathbb{R}^2$. The node $\mathbf{v}$ is connected to two vertices denoted by $\mathbf{v}'$ and $\mathbf{v}^\star$ in the cell C. We set $\mathcal{S}_{C,\mathbf{v}} = \{\mathbf{v}, \mathbf{v}', \mathbf{v}^\star\}$. Let us fix

$$x_{\sigma_{\mathbf{v}\mathbf{v}'}} = \frac{1}{2}(x_\mathbf{v} + x_{\mathbf{v}'}), \quad x_{\sigma_{\mathbf{v}\mathbf{v}^\star}} = \frac{1}{2}(x_\mathbf{v} + x_{\mathbf{v}^\star}), \tag{2.1}$$

and consider $d'_{C,\mathbf{v}} = \mathbf{dist}(\sigma_{\mathbf{v}\mathbf{v}^\star}, \sigma_{\mathbf{v}\mathbf{v}'})$. The unit normal (resp. tangent) vector to the edge

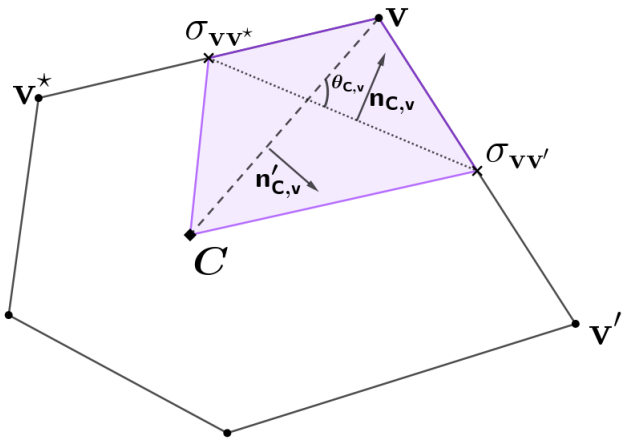

Figure 1: Configuration of a given cell C of the mesh $\mathcal{T}$. The embedded diamond $\mathcal{D}_{C,\mathbf{v}}$ is uniquely identified by C and the vertex $\mathbf{v}$.

$\sigma_{C\mathbf{v}} = [x_{\sigma_{\mathbf{v}\mathbf{v}^\star}}, x_{\sigma_{\mathbf{v}\mathbf{v}'}}]$ oriented from C to $\mathbf{v}$ (resp. $\sigma_{\mathbf{v}\mathbf{v}^\star}$ to $\sigma_{\mathbf{v}\mathbf{v}'}$) is denoted by $\mathbf{n}_{\mathbf{C},\mathbf{v}}$ (resp. $\mathbf{t}_{\mathbf{C},\mathbf{v}}$). In a similar way, one defines the unit vectors $\mathbf{n}'_{\mathbf{C},\mathbf{v}}$ and $\mathbf{t}'_{\mathbf{C},\mathbf{v}}$ corresponding to the edge $\sigma'_{C\mathbf{v}} = [x_C, x_\mathbf{v}]$ using the analogous orientation convention, depicted in Figure 1. The angle between $\mathbf{t}_{\mathbf{C},\mathbf{v}}$ and $\mathbf{t}'_{\mathbf{C},\mathbf{v}}$ is referred to as $\theta_{\mathbf{C},\mathbf{v}}$.

For each $\mathbf{v} \in \mathcal{S}_C$ we assign a sub-volume (triangle) $T_{C,\mathbf{v}} = C\sigma_{\mathbf{v}\mathbf{v}'}\sigma_{\mathbf{v}\mathbf{v}^\star}$ to the cell C. Similarly, the triangle $T'_{C,\mathbf{v}} = \sigma_{\mathbf{v}\mathbf{v}'}\mathbf{v}\sigma_{\mathbf{v}\mathbf{v}^\star}$ is attributed to the vertex $\mathbf{v}$. So, the sub-domain associated to the cell in question and its area read respectively

$$T_C = \bigcup_{\mathbf{v}\in\mathcal{S}_C} T_{C,\mathbf{v}}, \quad |T_C| = \sum_{\mathbf{v}\in\mathcal{S}_C} |T_{C,\mathbf{v}}|\,.$$

Analogously, the vertex volume with its area are respectively given by

$$T_\mathbf{v} = \bigcup_{C\in\mathcal{T}_\mathbf{v}} T'_{C,\mathbf{v}}, \quad |T_\mathbf{v}| = \sum_{C\in\mathcal{T}_\mathbf{v}} |T'_{C,\mathbf{v}}|\,.$$

By construction, it can be checked that

$$\overline{\Omega} = \Big(\bigcup_{C\in\mathcal{T}} \overline{T_C} \Big) \bigcup \Big(\bigcup_{\mathbf{v}\in\mathcal{S}} \overline{T_\mathbf{v}} \Big).$$

Let h_C be the diameter of C. The mesh size is given by $h_\mathcal{T} = \max_{C\in\mathcal{T}} h_C$. The analysis of the Node-Diamond scheme requires a standard regularity assumption on the mesh. In particular, its role is to prevent the cell degeneracy and to mostly keep the shape of the first element of the mesh sequence as $h_\mathcal{T}$ becomes very small. In other words, the number $\xi_\mathcal{M} = \max(\xi_\mathcal{T}, \xi_\mathcal{S})$ where

$$\xi_\mathcal{T} = \max_{C\in\mathcal{T}} \max_{\mathbf{v}\in\mathcal{S}_C} \left(\frac{1}{|\sin(\theta_{\mathbf{C},\mathbf{v}})|}, \frac{d_{C,\mathbf{v}}}{d'_{C,\mathbf{v}}}, \frac{h_C}{d_{C,\mathbf{v}}}, \frac{d_{C,\mathbf{v}}}{\sqrt{|T_{C,\mathbf{v}}|}}, \frac{d_{C,\mathbf{v}}}{\sqrt{|T'_{C,\mathbf{v}}|}}, \#\mathcal{S}_C \right), \quad \xi_\mathcal{S} = \max_{\mathbf{v}\in\mathcal{S}} \#\mathcal{T}_\mathbf{v},$$

needs to be uniformly bounded from above as the mesh size goes to 0.

We denote by $\mathbb{R}^\mathcal{M}$ the space composed of vectors $w_\mathcal{M}$ including the values of a variable w at the vertices and centers of cells, and having the form

$$w_\mathcal{M} = \big((w_\mathbf{v})_{\mathbf{v}\in\mathcal{S}}, (w_C)_{C\in\mathcal{T}} \big).$$

To conceive our approach we require an approximate gradient. To this end, consider the local basis $(\mathbf{t}_{\mathbf{C},\mathbf{v}}, \mathbf{t}'_{\mathbf{C},\mathbf{v}})$. Define the diamond region $\mathcal{D}_{C,\mathbf{v}} = C\sigma_{\mathbf{v}\mathbf{v}'}\mathbf{v}\sigma_{\mathbf{v}\mathbf{v}^\star}$ on which we build a discrete gradient satisfying the two-point relationships

$$\nabla_{\mathcal{D}_{C,\mathbf{v}}} w_\mathcal{M} \cdot \mathbf{t}_{\mathbf{C},\mathbf{v}} = \frac{w_\mathbf{v} - w_C}{d_{C,\mathbf{v}}}, \qquad \nabla_{\mathcal{D}_{C,\mathbf{v}}} w_\mathcal{M} \cdot \mathbf{t}'_{\mathbf{C},\mathbf{v}} = \frac{w_{\sigma_{\mathbf{v}\mathbf{v}'}} - w_{\sigma_{\mathbf{v}\mathbf{v}^\star}}}{d'_{C,\mathbf{v}}},$$

necessitated for consistency reasons. These discrete directional derivatives allow to equivalently get

$$\nabla_{\mathcal{D}_{C,\mathbf{v}}} w_\mathcal{M} = \frac{1}{\sin(\theta_{\mathbf{C},\mathbf{v}})} \Big(\frac{w_\mathbf{v} - w_C}{d_{C,\mathbf{v}}} \mathbf{n}_{\mathbf{C},\mathbf{v}} + \frac{w_{\sigma_{\mathbf{v}\mathbf{v}'}} - w_{\sigma_{\mathbf{v}\mathbf{v}^\star}}}{d'_{C,\mathbf{v}}} \mathbf{n}'_{\mathbf{C},\mathbf{v}} \Big).$$

We would like to avoid storing edge unknowns per each cell, which can be expensive from the implementation viewpoint. To this purpose, we use the interpolations (2.1) to express $w_{\sigma_{\mathbf{v}\mathbf{v}'}}, w_{\sigma_{\mathbf{v}\mathbf{v}^\star}}$ in terms of the C-cell vertices connected to $\mathbf{v}$. Therefore, this gives rise to a novel interpolated gradient on the same diamond sub-set $\mathcal{D}_{C,\mathbf{v}}$ that is now written as

$$\nabla_{\mathcal{D}_{C,\mathbf{v}}} w_\mathcal{M} = \frac{1}{\sin(\theta_{\mathbf{C},\mathbf{v}})} \Big(\frac{w_\mathbf{v} - w_C}{d_{C,\mathbf{v}}} \mathbf{n}_{\mathbf{C},\mathbf{v}} + \frac{1}{2} \frac{w_{\mathbf{v}'} - w_{\mathbf{v}^\star}}{d'_{C,\mathbf{v}}} \mathbf{n}'_{\mathbf{C},\mathbf{v}} \Big). \tag{2.2}$$

Notice that $|\mathcal{D}_{C,\mathbf{v}}| = d_{C,\mathbf{v}} d'_{C,\mathbf{v}} \sin(\theta_{\mathbf{C},\mathbf{v}})/2$. Accordingly, one has

$$\nabla_{\mathcal{D}_{C,\mathbf{v}}} w_\mathcal{M} = \frac{1}{2\,|\mathcal{D}_{C,\mathbf{v}}|} \Big(d'_{C,\mathbf{v}} \,(w_\mathbf{v} - w_C)\, \mathbf{n}_{\mathbf{C},\mathbf{v}} + \frac{1}{2} d_{C,\mathbf{v}} \,(w_{\mathbf{v}'} - w_{\mathbf{v}^\star})\, \mathbf{n}'_{\mathbf{C},\mathbf{v}} \Big).$$

The proposed numerical scheme will thereby rely on this special gradient formula (2.2).

Motivated by applications such as the modeling of flows through heterogeneous porous media, the (permeability) tensor κ is approximated piecewisely in each cell using the averaged integral

$$\kappa_C = \frac{1}{|C|} \int_C \kappa(x)\, \mathrm{d}x. \tag{2.3}$$

Note that $\kappa(x)$ is not necessarily continuous within Ω and it could be discontinuous across the edges of C. To approximate the source term we take advantage of the standard means on the volumes T_C and $T_\mathbf{v}$ as follows

$$f_{T_C} = \frac{1}{|T_C|} \int_{T_C} f(x)\, \mathrm{d}x, \quad f_{T_\mathbf{v}} = \frac{1}{|T_\mathbf{v}|} \int_{T_\mathbf{v}} f(x)\, \mathrm{d}x.$$

For simplicity of the numerical analysis, since our study focuses on the design of the Node-Diamond scheme and its properties, we assume that $g \in H^1(\Omega)$ to avoid discussions related to the reconstruction of the boundary data at the discrete level. Using the guidelines of [6], the results of our methodology are still valid in the general case with $g \in H^{1/2}(\partial\Omega)$. Since $g \in H^1(\Omega)$, define the discrete boundary data as done for the source term

$$g_{T_C} = \frac{1}{|T_C|}\int_{T_C} g(x)\,\mathrm{d}x, \quad g_{T_\mathbf{v}} = \frac{1}{|T_\mathbf{v}|}\int_{T_\mathbf{v}} g(x)\,\mathrm{d}x.$$

We introduce the discrete spaces

$$X_{\mathcal{M},g} = \{w_\mathcal{M} \in \mathbb{R}^\mathcal{M} \,:\, w_\mathbf{v} = g_{T_\mathbf{v}}, \quad \forall \mathbf{v} \in \mathcal{S}^D\}, \quad X_{\mathcal{M},0} = \{w_\mathcal{M} \in \mathbb{R}^\mathcal{M} \,:\, w_\mathbf{v} = 0, \quad \forall \mathbf{v} \in \mathcal{S}^D\}.$$

Define the discrete semi-norms on $X_{\mathcal{M},g}$

$$\|w_\mathcal{M}\|_0 = \left(\sum_{C\in\mathcal{T}} |T_C|\, w_C^2 + \sum_{\mathbf{v}\in\mathcal{S}} |T_\mathbf{v}|\, w_\mathbf{v}^2\right)^{1/2}, \quad \|u_\mathcal{M}\|_1 = \left(\sum_{C\in\mathcal{T}}\sum_{\mathbf{v}\in\mathcal{S}_C} |\mathcal{D}_{C,\mathbf{v}}|\left|\nabla_{\mathcal{D}_{C,\mathbf{v}}} w_\mathcal{M}\right|^2\right)^{1/2}.$$

The following statement is referred to as the discrete Poincaré's inequality. More interestingly, it ensures that $\|\cdot\|_1$ is indeed a norm on $X_{\mathcal{M},0}$.

Lemma 2.1. *There exists $B_p > 0$ depending only on the mesh regularity and Ω such that*

$$\|w_\mathcal{M}\|_0 \le B_p \|w_\mathcal{M}\|_1, \quad \forall w_\mathcal{M} \in X_{\mathcal{M},0}.$$

Proof. Let $w_\mathcal{M} \in X_{\mathcal{M},0}$. Following [6, 19], there exists a positive constant B which depends only on the diameter of Ω such that

$$\|w_\mathcal{M}\|_0^2 = \sum_{K\in\mathcal{M}} |T_K|\,|w_K|^2 \le B \sum_{C\in\mathcal{T}}\sum_{\mathbf{v}\in\mathcal{S}_C} d_{C,\mathbf{v}} d'_{C,\mathbf{v}} \frac{|w_C - w_\mathbf{v}|}{d'_{C,\mathbf{v}}}\big(|u_C| + |u_\mathbf{v}|\big).$$

The mesh regularity claims that

$$d_{C,\mathbf{v}} d'_{C,\mathbf{v}} \le B' |\mathcal{D}_{C,\mathbf{v}}|, \quad d_{C,\mathbf{v}} d'_{C,\mathbf{v}} \le B' |T_C|, \quad d_{C,\mathbf{v}} d'_{C,\mathbf{v}} \le B' |T_\mathbf{v}|,$$

for some constant $B' > 0$. Accordingly, we use the Cauchy-Schwarz inequality and arrange the terms of each summation to finally obtain

$$\begin{aligned}\|w_\mathcal{M}\|_0^2 &\le B'' \sum_{C\in\mathcal{T}}\sum_{\mathbf{v}\in\mathcal{S}_C} |\mathcal{D}_{C,\mathbf{v}}| \left|\frac{w_C - w_\mathbf{v}}{d'_{C,\mathbf{v}}}\right|^2 \\ &\le B'' \sum_{C\in\mathcal{T}}\sum_{\mathbf{v}\in\mathcal{S}_C} |\mathcal{D}_{C,\mathbf{v}}| \left|\nabla_{\mathcal{D}_{C,\mathbf{v}}} w_\mathcal{M} \cdot \mathbf{t}_{\mathbf{C},\mathbf{v}}\right|^2 \le B'' \|w_\mathcal{M}\|_1^2,\end{aligned}$$

as required. This concludes the proof. □

Let $\mathcal{I}_\mathcal{M}$ be the function reconstruction operator defined from $X_{\mathcal{M},g}$ into $L^2(\Omega)$ by

$$\mathcal{I}_\mathcal{M} w_\mathcal{M} = \sum_{K\in\mathcal{M}} |T_K|\, w_K \chi_K,$$

where χ_K is the characteristic function on K. For shortness, we will adopt the notation $w_h = \mathcal{I}_\mathcal{M} w_\mathcal{M}$. Similarly, the discrete gradient is the linear operator ∇_h mapping $X_{\mathcal{M},g}$ into $L^2(\Omega)^2$ and defined as follows

$$\nabla_h w_\mathcal{M} := \sum_{C\in\mathcal{T}}\sum_{\mathbf{v}\in\mathcal{S}_C} \nabla_{\mathcal{D}_{C,\mathbf{v}}} w_\mathcal{M} \chi_{\mathcal{D}_{C,\mathbf{v}}}.$$

We will also need the reconstruction of the diffusion tensor that we define in the same manner on the mesh cells as

$$\kappa_{h,\mathcal{T}} := \sum_{C\in\mathcal{T}} |C|\, \kappa_C \chi_C.$$

These preliminaries and notations are useful to describe the proposed nodal scheme discretization in the subsequent section.

3 Node-Diamond numerical scheme

Here, we describe the principle of the proposed discretization method for the elliptic model problem (1.1)-(1.2). Given the key definition of the discrete gradient operator, the Node-Diamond scheme is founded on a discrete counterpart of the "variational formulation", which consists of finding $u_{\mathcal{M}} \in X_{\mathcal{M},g}$ that solves the problem

$$a_h(u_{\mathcal{M}}, \varphi_{\mathcal{M}}) := \int_\Omega \kappa_{h,\mathcal{T}} \nabla_h u_{\mathcal{M}} \cdot \nabla_h \varphi_{\mathcal{M}} \, \mathrm{d}x = \int_\Omega f \varphi_h \, \mathrm{d}x, \quad \forall \varphi_{\mathcal{M}} \in X_{\mathcal{M},0}. \tag{3.1}$$

The compact formulation (3.1) is quite helpful to carry out the scheme analysis. Some details on the practical implementation of the Node-Diamond scheme are given in the numerical section.

Notice that the cell equation is obtained by taking $\varphi_{\mathcal{M}} = \mathbf{1}_C$ in (3.1). Here $\mathbf{1}_C$ denotes the C-th vector of the canonical basis of $\mathbb{R}^{\mathcal{M}}$. Similarly, the vertex equation is derived by selecting $\varphi_{\mathcal{M}} = \mathbf{1}_{\mathbf{v}}$ in (3.1). Therefore, we obtain the proposed Node-Diamond scheme on each cell volume T_C and vertex volume $T_{\mathbf{v}}$

$$\sum_{\mathbf{v} \in \mathcal{S}_C} |\mathcal{D}_{C,\mathbf{v}}| \, \kappa_C \nabla_{\mathcal{D}_{C,\mathbf{v}}} u_{\mathcal{M}} \cdot \nabla_{\mathcal{D}_{C,\mathbf{v}}} \mathbf{1}_C = |T_C| \, f_{T_C} \quad \forall C \in \mathcal{T}, \tag{3.2}$$

$$\sum_{C \in \mathcal{T}_{\mathbf{v}}} \sum_{\nu \in \mathcal{S}_{C,\mathbf{v}}} |\mathcal{D}_{C,\mathbf{v}}| \, \kappa_C \nabla_{\mathcal{D}_{C,\nu}} u_{\mathcal{M}} \cdot \nabla_{\mathcal{D}_{C,\nu}} \mathbf{1}_{\mathbf{v}} = |T_{\mathbf{v}}| \, f_{T_{\mathbf{v}}} \quad \forall \mathbf{v} \in \mathcal{S} \setminus \mathcal{S}^D. \tag{3.3}$$

Due to the Dirichlet boundary condition (1.2), it is imposed that

$$u_{\mathbf{v}} = g_{\mathbf{v}}, \quad \forall \mathbf{v} \in \mathcal{S}^D. \tag{3.4}$$

We note that

$$|\mathcal{D}_{C,\mathbf{v}}| \, \kappa_C \nabla_{\mathcal{D}_{C,\mathbf{v}}} u_{\mathcal{M}} \cdot \nabla_{\mathcal{D}_{C,\mathbf{v}}} \mathbf{1}_C = \alpha_{C\mathbf{v}} (u_C - u_{\mathbf{v}}) + \beta_{C\mathbf{v}} (u_{\mathbf{v}^\star} - u_{\mathbf{v}'}),$$

where

$$\alpha_{C\mathbf{v}} = \frac{1}{2\,|\mathcal{D}_{C,\mathbf{v}}|} (d'_{C,\mathbf{v}})^2 \kappa_C \mathbf{n}_{\mathbf{C},\mathbf{v}} \cdot \mathbf{n}_{\mathbf{C},\mathbf{v}}, \quad \beta_{C\mathbf{v}} = \frac{1}{4\,|\mathcal{D}_{C,\mathbf{v}}|} d_{C,\mathbf{v}} d'_{C,\mathbf{v}} \kappa_C \mathbf{n}_{\mathbf{C},\mathbf{v}} \cdot \mathbf{n}'_{\mathbf{C},\mathbf{v}}.$$

The previous relationship claims that the information exchange mainly occurs between the cell and its vertices. Accordingly, as will be shown in the numerical section, the cell unknowns can be eliminated without any fill-in at the solver level since they only depend on the surrounding vertex unknowns. Therefore, the computational cost is strongly linked to the total number of the mesh nodes. This feature is one of the main assets of our contribution.

Remark 3.1. *Given a scalar diffusion tensor κ, the Node-Diamond scheme (3.2)-(3.4) can be monotone in some circumstances. First, it concisely rewritten under the linear matrix form $\boldsymbol{A} u_{\mathcal{M}} = \mathbf{b}_{\mathcal{M}}$ where more details on the assembling are given in the numerical section. When all $\beta_{C\mathbf{v}}$ are zero, meaning that $\sigma_{C\mathbf{v}}$ and $\sigma'_{C\mathbf{v}}$ are perpendicular, the stiffness matrix $\boldsymbol{A}$ has the M-matrix structure. For instance, this is achieved on meshes composed of squares, equilateral triangulations and rhombuses with identical edges.*

3.1 Case of additional convection

It is quite natural to wonder if the proposed Node-Diamond scheme can be extended to the context of convection-diffusion problems of the form

$$-\nabla \cdot \kappa(x) \nabla u + \nabla \cdot u\mathbf{q} = f \quad \text{in } \Omega, \tag{3.5}$$

$$u = g \quad \text{on } \partial\Omega, \tag{3.6}$$

where $\mathbf{q}$ is the velocity vector that should be in $\mathcal{C}^1(\overline{\Omega}, \mathbb{R}^2)$ and satisfy $\nabla \cdot \mathbf{q} \geq 0$. The response to this quest is positive. Indeed, it is suffices to treat the transport term in the same spirit of the

finite volume methodology by considering that T_C and $T_{\mathbf{v}}$ play the role of the control volumes. Such a strategy is widely used in the literature. For instance, we mention the combination of the finite elements and the finite volumes [5, 22, 23, 27]. More precisely, the finite element method is concerned with the discretization of the diffusion and the finite volume approach yields the approximation of the advection. Also, in [12] the authors showed how to discretize the convective term in the case of multi-point methods, notably hybrid mimetic mixed methods, using a couple of finite volume schemes. As the Node-Diamond scheme belongs the family of multi-point methods, it is possible to adapt the technique of [12] for our case as follows. First, denote by $(\sigma_{\mathbf{v}\mathbf{v}'}, \sigma_{\mathbf{v}\mathbf{v}^\star})$ the line crossing $\sigma_{\mathbf{v}\mathbf{v}'}$ and $\sigma_{\mathbf{v}\mathbf{v}^\star}$. Let us define

$$o_{C,\mathbf{v}} = \mathbf{dist}\Big(C, (\sigma_{\mathbf{v}\mathbf{v}'}, \sigma_{\mathbf{v}\mathbf{v}^\star})\Big) + \mathbf{dist}\Big(\mathbf{v}, (\sigma_{\mathbf{v}\mathbf{v}'}, \sigma_{\mathbf{v}\mathbf{v}^\star})\Big).$$

At the interface between the adjacent volumes T_C and $T_{\mathbf{v}}$, we approximate the velocity field by

$$\mathbf{q}_{C,\mathbf{v}} = \frac{1}{d'_{C,\mathbf{v}}} \int_{\sigma_{C,\mathbf{v}}} \mathbf{q} \cdot \mathbf{n}_{\mathbf{C},\mathbf{v}} \, \mathrm{d}s.$$

Given a specific function μ_C, that will be described below, the advective contribution is fully discretized using the following coefficients

$$\boldsymbol{\mu}_{\boldsymbol{C}\mathbf{v}} = \frac{d'_{C,\mathbf{v}}}{o_{C,\mathbf{v}}} \mu_C \left(o_{C,\mathbf{v}} \mathbf{q}_{C,\mathbf{v}}\right), \quad \boldsymbol{\mu}_{\mathbf{v}\boldsymbol{C}} = \frac{d'_{C,\mathbf{v}}}{o_{C,\mathbf{v}}} \mu_C \left(-o_{C,\mathbf{v}} \mathbf{q}_{C,\mathbf{v}}\right).$$

Accordingly, the Node-Diamond scheme for steady convection-diffusion problems is written as

$$\sum_{\mathbf{v}\in\mathcal{S}_C} |\mathcal{D}_{C,\mathbf{v}}| \, \kappa_C \nabla_{\mathcal{D}_{C,\mathbf{v}}} u_{\mathcal{M}} \cdot \nabla_{\mathcal{D}_{C,\mathbf{v}}} \mathbf{1}_C + \sum_{\mathbf{v}\in\mathcal{S}_C} \left(\boldsymbol{\mu}_{\mathbf{v}\boldsymbol{C}} u_C - \boldsymbol{\mu}_{\boldsymbol{C}\mathbf{v}} u_{\mathbf{v}}\right) = |T_C| \, f_{T_C} \quad \forall C \in \mathcal{T}, \tag{3.7}$$

$$\sum_{C\in\mathcal{T}_{\mathbf{v}}} \sum_{\nu\in\mathcal{S}_{C,\mathbf{v}}} |\mathcal{D}_{C,\mathbf{v}}| \, \kappa_C \nabla_{\mathcal{D}_{C,\nu}} u_{\mathcal{M}} \cdot \nabla_{\mathcal{D}_{C,\nu}} \mathbf{1}_{\mathbf{v}} - \sum_{C\in\mathcal{T}_{\mathbf{v}}} \alpha_{C\mathbf{v}} \big(\boldsymbol{\mu}_{\mathbf{v}\boldsymbol{C}} u_C - \boldsymbol{\mu}_{\boldsymbol{C}\mathbf{v}} u_{\mathbf{v}}\big) = |T_{\mathbf{v}}| \, f_{T_{\mathbf{v}}} \quad \forall \mathbf{v} \in \mathcal{S} \setminus \mathcal{S}^D, \tag{3.8}$$

$$u_{\mathbf{v}} = g_{\mathbf{v}}, \quad \forall \mathbf{v} \in \mathcal{S}^D. \tag{3.9}$$

We now indicate two possible choices of the function μ_C.

(i) **Upwind scheme** : the upwind scheme amounts to setting $\mu_C(a) = \max(a, 0)$. Its stability is ensured at the price of additional excessive numerical diffusion. It turns out that the artificial viscosity is not necessary in the diffusive regime can and be automatically controlled using the Scharfetter–Gummel technique.

(ii) **Scharfetter–Gummel scheme** : the Scharfetter–Gummel discretization [31] behaves better than the upwind scheme in regions where diffusion is dominant. For large Péclet numbers, it is numerically equivalent to the upwind scheme in the sense that they provide similar convergence rates. Following [12], the convective flux approximation is given by

$$\mu_C(a) = \min(1, \lambda_{\kappa_C}) \mu_{\mathrm{sg}} \left(\frac{a}{\min(1, \lambda_{\kappa_C})}\right), \quad \mu_{\mathrm{sg}}(s) = \frac{-s}{e^{-s} - 1} - 1, \; s \neq 0, \; \mu_{\mathrm{sg}}(0) = 0.$$

The scalar λ_{κ_C} is nothing more than the smallest eigenvalue of κ_C. The scaling factor $\min(1, \lambda_{\kappa_C})$ is required to maintain the stability of the scheme. See also [30] for a different Scharfetter–Gummel approach elaborated in the framework of discrete duality finite volume methods.

We stress that all the theoretical results, of the present paper, are still valid in the presence of convection. It is handled with no difficult technicalities as already done in the literature [12]. For this reason, we omit to include the advective term in the analysis below.

3.2 Coercivity and existence of the discrete solution

In this part, we are going to establish the energy estimate on the solution. We also prove the existence and uniqueness of the numerical solution.

First, the following result shows that any solution of the finite volume scheme is uniformly bounded with respect to the semi-norm $\|\cdot\|_1$.

Proposition 3.1. *The numerical scheme (3.2)-(3.4) is coercive in the sense that there exists a positive constant B depending only on g, $\underline{\kappa}$, $\overline{\kappa}$, f, Ω, and the mesh regularity such that*

$$\|u_{\mathcal{M}}\|_1 \leq B. \tag{3.10}$$

Proof. Taking $\varphi_{\mathcal{M}} = u_{\mathcal{M}} - g_{\mathcal{M}} \in X_{\mathcal{M},0}$ in the discrete weak formulation (3.1) yields

$$X_1 = X_2 + X_3,$$

where

$$X_1 = \int_\Omega \kappa_{h,\mathcal{T}} \nabla_h u_{\mathcal{M}} \cdot \nabla_h u_{\mathcal{M}} \,\mathrm{d}x, \quad X_2 = \int_\Omega \kappa_{h,\mathcal{T}} \nabla_h u_{\mathcal{M}} \cdot \nabla_h g_{\mathcal{M}} \,\mathrm{d}x,$$
$$X_3 = \int_\Omega f\big(u_h - g_h\big) \,\mathrm{d}x.$$

The ellipticity of the tensor κ and the definition of the discrete semi-norm $\|\cdot\|_1$ imply

$$X_1 \geq \underline{\kappa} \|u_{\mathcal{M}}\|_1^2 .$$

A straightforward adaptation of the interpolation result [6, Lemma 3.5] leads to

$$\|g_{\mathcal{M}}\|_1 \leq B_0 \|g\|_{H^1(\Omega)} ,$$

where B_0 depends only on the mesh regularity. As a result, we use the Cauchy-Schwarz, and Young's inequalities to get

$$|X_2| \leq \frac{\underline{\kappa}}{4} \|u_{\mathcal{M}}\|_1^2 + \frac{\overline{\kappa}}{\underline{\kappa}} \|g_{\mathcal{M}}\|_1^2 \leq \frac{\underline{\kappa}}{4} \|u_{\mathcal{M}}\|_1^2 + \frac{\overline{\kappa} B_0^2}{\underline{\kappa}} \|g\|_{H^1(\Omega)}^2 .$$

We proceed as above and make use of Poincaré's inequality to find

$$\begin{aligned} |X_3| &\leq B_p \|f\|_{L^2(\Omega)} \|u_{\mathcal{M}} - g_{\mathcal{M}}\|_1 \\ &\leq \frac{\underline{\kappa}}{4} \|u_{\mathcal{M}}\|_1^2 + \frac{B_p^2}{\underline{\kappa}} \|f\|_{L^2(\Omega)}^2 + B_p B_0 \|f\|_{L^2(\Omega)} \|g\|_{H^1(\Omega)} . \end{aligned}$$

Gathering these estimations we deduce $\|u_{\mathcal{M}}\|_1 \leq B$ where

$$B = \Big(2\overline{\kappa} B_0^2 \|g\|_{H^1(\Omega)}^2 + 2B_p^2 \|f\|_{L^2(\Omega)}^2 + 2\underline{\kappa} B_p B_0 \|f\|_{L^2(\Omega)} \|g\|_{H^1(\Omega)} \Big)^{1/2} .$$

This finishes the proof. □

Next, we prove the existence and uniqueness of the numerical solution.

Proposition 3.2. *There exists a unique solution to the Node-Diamond scheme (3.2)-(3.4).*

Proof. Let $Pg_{\mathcal{M}}$ be the orthogonal projection of $g_{\mathcal{M}} \in X_{\mathcal{M},g}$ on the sub-space $X_{\mathcal{M},0}$. Set $\widehat{g}_{\mathcal{M}} = g_{\mathcal{M}} - Pg_{\mathcal{M}}$. Perform the change of variables $w_{\mathcal{M}} = u_{\mathcal{M}} - \widehat{g}_{\mathcal{M}}$. Thus, the numerical scheme (3.2)-(3.4) rewrites

$$\begin{array}{lll} a_h(w_{\mathcal{M}}, \mathbf{1}_C) & = |T_C| \, f_{T_C} - a_h(\widehat{g}_{\mathcal{M}}, \mathbf{1}_C), & \forall C \in \mathcal{T}, \\ a_h(w_{\mathcal{M}}, \mathbf{1}_{\mathbf{v}}) & = |T_{\mathbf{v}}| \, f_{T_{\mathbf{v}}} - a_h(\widehat{g}_{\mathcal{M}}, \mathbf{1}_{\mathbf{v}}), & \forall \mathbf{v} \in \mathcal{S} \setminus \mathcal{S}^D, \\ w_{\mathbf{v}} & = 0, & \forall \mathbf{v} \in \mathcal{S}^D. \end{array} \tag{3.11}$$

Let us set $\mathcal{M}^\star = \mathcal{M} \setminus \mathcal{S}^D$. Observe that $w_{\mathcal{M}^\star} = u_{\mathcal{M}^\star}$. The linear system (3.11) can be recast under the matrix form $\mathcal{A}u_{\mathcal{M}^\star} = \mathcal{F}_{\mathcal{M}^\star}$, where the coefficients of the matrix $\mathcal{A}$ and those of the second member $\mathcal{F}_{\mathcal{M}^\star}$ are given by

$$\begin{cases} \mathcal{A}_{ij} = a_h(\mathbf{1}_i, \mathbf{1}_j) & \text{for} \quad 1 \le i,j \le \#\mathcal{M}^\star, \\ \mathcal{F}_i = |T_i|\, f_{T_i} - a_h(\widehat{g}_{\mathcal{M}}, \mathbf{1}_i) & \text{for} \quad 1 \le i \le \#\mathcal{M}^\star. \end{cases}$$

The right hand side $\mathcal{F}_{\mathcal{M}^\star}$ is fully known. The existence and the uniqueness of the numerical solution to (3.2)-(3.4) is equivalent to showing that the kernel of $\mathcal{A}$ is trivial. Let us then prove that $\mathrm{Ker}(\mathcal{A}) = \{0_{\mathcal{M}^\star}\}$. Let $v_{\mathcal{M}^\star} \in \mathrm{Ker}(\mathcal{A})$. Thereby, $\mathcal{A}v_{\mathcal{M}^\star} = 0_{\mathcal{M}^\star}$ which implies that $\mathcal{A}v_{\mathcal{M}^\star} \cdot v_{\mathcal{M}^\star} = 0$. Next, owing to the definition of the matrix $\mathcal{A}$ and the expression of the bilinear form a_h defined in (3.1) we infer

$$0 = \mathcal{A}v_{\mathcal{M}^\star} \cdot v_{\mathcal{M}^\star} = a_h(v_{\mathcal{M}^\star}, v_{\mathcal{M}^\star}) \ge \underline{\kappa}\, \|v_{\mathcal{M}^\star}\|_1^2 .$$

Recall that $\|\cdot\|_1$ is a norm on $X_{\mathcal{M},0}$ thanks to Poincaré's inequality. Accordingly $v_{\mathcal{M}^\star} = 0_{\mathcal{M}^\star}$ and this leads to $\mathrm{Ker}(\mathcal{A}) = \{0_{\mathcal{M}^\star}\}$, which establishes that $\mathcal{A}$ is invertible. As a consequence, $u_{\mathcal{M}^\star} = \mathcal{A}^{-1}\mathcal{F}$. The proof is concluded. □

3.3 Convergence analysis

In this last subsection we focus on the convergence analysis of the Node-Diamond scheme and the passage to the limit. This is conducted by means of compactness.

Lemma 3.1. *Let $v_{\mathcal{M}} \in X_{\mathcal{M},0}$. The reconstruction function v_h is naturally extended by 0 outside of Ω. Then, there exists a positive constant B depending only on the mesh regularity such that*

$$||v_h(\cdot + \boldsymbol{y}) - v_h||_{L^1(\mathbb{R}^2)} \le B\,|\boldsymbol{y}|\,||v_{\mathcal{M}}||_1, \quad \forall \boldsymbol{y} \in \mathbb{R}^2. \tag{3.12}$$

Proof. Fix $\mathbf{y} \in \mathbb{R}^2$ and let $x \in \mathbb{R}^2$. In the same spirit of the proof made in [6, Lemma 3.8], define the edge identification function

$$\eta_{C,\mathbf{v}}(x,\mathbf{y}) = \begin{cases} 1, & \text{if } [\sigma_{\mathbf{v}\mathbf{v}^\star}, \sigma_{\mathbf{v}\mathbf{v}'}] \cap [x+\mathbf{y}, x] \neq \emptyset, \\ 0, & \text{else.} \end{cases}$$

Then, for all $x \in \mathbb{R}^2$, there holds

$$|v_h(x+\mathbf{y}) - v_h(x)| \le \sum_{C\in\mathcal{T}} \sum_{\mathbf{v}\in\mathcal{S}_C} \eta_{C,\mathbf{v}}(x,\mathbf{y})\,|v_{\mathbf{v}} - v_C| \le \sum_{C\in\mathcal{T}} \sum_{\mathbf{v}\in\mathcal{S}_C} \eta_{C,\mathbf{v}}(x,\mathbf{y}) d_{C,\mathbf{v}} \frac{|u_{\mathbf{v}} - u_C|}{d_{C,\mathbf{v}}}.$$

It can be checked that

$$\int_{\mathbb{R}^2} \eta_{C,\mathbf{v}}(x,\mathbf{y})\,\mathrm{d}x \le d'_{C,\mathbf{v}}\,|\mathbf{y}|\,.$$

As a consequence of this and the Cauchy-Schwarz inequality, one gets

$$||v_h(\cdot+\mathbf{y}) - v_h||_{L^1(\mathbb{R}^2)} \le B'\,|\mathbf{y}| \sum_{C\in\mathcal{T}} \sum_{\mathbf{v}\in\mathcal{S}_C} |\mathcal{D}_{C,\mathbf{v}}|\,\left|\nabla_{\mathcal{D}_{C,\mathbf{v}}} w\right| \le B\,|\mathbf{y}|\,\|v_{\mathcal{M}}\|_1\,.$$

where the constants B' and B depend only on the mesh regularity. The proof is complete. □

In the sequel, we denote B_i a finite series of positive constants depending only on the data and possibly on the mesh regularity. In the following result, we state and prove the convergence theorem for the Node-Diamond numerical scheme.

Theorem 3.1. *Let $(\mathcal{M}_\ell)_{\ell\in\mathbb{N}}$ be a sequence of meshes such that $\xi_{\mathcal{M}_\ell}$ is uniformly bounded and $h_{\mathcal{M}_\ell}$ goes to 0 as $\ell\to+\infty$. Then*

$$g_{h_\ell} \xrightarrow[\ell\to+\infty]{} g \text{ strongly in } H^1(\Omega), \tag{3.13}$$

and there exists $u\in H^1(\Omega)$ such that

$$\begin{aligned} u_{h_\ell} &\xrightarrow[\ell\to+\infty]{} u && \text{strongly in } L^2(\Omega),\\ \nabla_{h_\ell} u_{\mathcal{M}_\ell} &\xrightarrow[\ell\to+\infty]{} \nabla u && \text{weakly in } L^2(\Omega)^2, \end{aligned} \tag{3.14}$$

up to the extraction of a subsequence. In addition, u is the unique weak solution to the variational formulation (1.4). Therefore, the convergence holds for the whole sequence. Finally, a better convergence is valid for the gradient of the numerical solution sequence i.e.

$$\nabla_{h_\ell} u_{\mathcal{M}_\ell} \xrightarrow[\ell\to+\infty]{} \nabla u \text{ strongly in } L^2(\Omega)^2. \tag{3.15}$$

Proof. First, the strong convergence (3.13) is obtained by mimicking the guidelines of [6, Proposition 3.6, Corollary 3.7]. Set $v_{\mathcal{M}_\ell} = u_{\mathcal{M}_\ell} - g_{\mathcal{M}_\ell}$. Then $v_{\mathcal{M}_\ell}\in X_{\mathcal{M}_\ell,0}$. By virtue of Lemma 3.1 and Kolmogorov's compactness criterion, there exists $v\in L^1(\Omega)$ such that

$$v_{h_\ell} \xrightarrow[\ell\to+\infty]{} v \quad \text{strongly in } L^1(\Omega),$$

up to a subsequence. Using the result [17, Lemma B.15], one can check that the sequence $(v_{h_\ell})_{\ell\in\mathbb{N}}$ is bounded in $L^q(\Omega)$ for some $q>2$ independently of the mesh size. An adaptation of the proof established for [17, Lemma B.19] yields that $(v_{h_\ell})_{\ell\in\mathbb{N}}$ is relatively compact in $L^2(\Omega)$. Therefore, introduce (3.13) to see that the first convergence of (3.14) holds true.

Th estimate (3.10) implies the existence of some $\mathbf{G}\in L^2(\Omega)^2$ such that

$$\nabla_{h_\ell} v_{\mathcal{M}_\ell} \xrightarrow[\ell\to+\infty]{} \mathbf{G} \text{ weakly in } L^2(\Omega)^2.$$

Let us now demonstrate the identification of the limit i.e. $\mathbf{G}=\nabla v$ a.e. in Ω for the Node-Diamond scheme. Take $\psi\in\mathcal{C}_c^\infty(\Omega)^2$. We denote by A_ℓ the integral

$$A_\ell = \int_\Omega \nabla_{h_\ell} v_{\mathcal{M}_\ell}\cdot\psi\,\mathrm{d}x + \int_\Omega v_{h_\ell}\nabla\cdot\psi\,\mathrm{d}x.$$

Using the weak convergence of $\left(\nabla_{h_\ell} v_{\mathcal{M}_\ell}\right)_\ell$ and the strong one of $(v_{\mathcal{M}_\ell})_\ell$ we obtain

$$A_\ell \xrightarrow[\ell\to+\infty]{} \int_\Omega \mathbf{G}\cdot\psi\,\mathrm{d}x + \int_\Omega v\nabla\cdot\psi\,\mathrm{d}x.$$

Following [6], we define

$$\psi_{\mathcal{D}_{C,\mathbf{v}}} = \frac{1}{|\mathcal{D}_{C,\mathbf{v}}|}\int_{\mathcal{D}_{C,\mathbf{v}}}\psi(x)\,\mathrm{d}x,\quad \psi_{\sigma_{C,\mathbf{v}}} = \frac{1}{d'_{C,\mathbf{v}}}\int_{\sigma_{C,\mathbf{v}}}\psi(s)\,\mathrm{d}s,\quad \psi_{\sigma'_{C,\mathbf{v}}} = \frac{1}{d_{C,\mathbf{v}}}\int_{\sigma'_{C,\mathbf{v}}}\psi(s)\,\mathrm{d}s.$$

Let us consider the vector $\widetilde{\psi}_{\mathcal{D}_{C,\mathbf{v}}}$ of $\mathbb{R}^2$ uniquely defined by

$$\widetilde{\psi}_{\mathcal{D}_{C,\mathbf{v}}}\cdot\mathbf{n}_{\mathbf{C},\mathbf{v}} = \psi_{\sigma_{C,\mathbf{v}}}\cdot\mathbf{n}_{\mathbf{C},\mathbf{v}},\quad \widetilde{\psi}_{\mathcal{D}_{C,\mathbf{v}}}\cdot\mathbf{n}'_{\mathbf{C},\mathbf{v}} = \psi_{\sigma'_{C,\mathbf{v}}}\cdot\mathbf{n}'_{\mathbf{C},\mathbf{v}}.$$

The first integral of A_ℓ is split as follows

$$\begin{aligned}\int_\Omega \nabla_{h_\ell} v_{\mathcal{M}_\ell}\cdot\psi\,\mathrm{d}x := Y_\ell + Z_\ell = &\sum_{C\in\mathcal{T}_\ell}\sum_{\mathbf{v}\in\mathcal{S}_C}|\mathcal{D}_{C,\mathbf{v}}|\,\nabla_{\mathcal{D}_{C,\mathbf{v}}} v_{\mathcal{M}_\ell}\cdot\widetilde{\psi}_{\mathcal{D}_{C,\mathbf{v}}}\\ &+\sum_{C\in\mathcal{T}_\ell}\sum_{\mathbf{v}\in\mathcal{S}_C}|\mathcal{D}_{C,\mathbf{v}}|\,\nabla_{\mathcal{D}_{C,\mathbf{v}}} v_{\mathcal{M}_\ell}\cdot\left(\psi_{\mathcal{D}_{C,\mathbf{v}}}-\widetilde{\psi}_{\mathcal{D}_{C,\mathbf{v}}}\right).\end{aligned}$$

Observe that $\|v_{\mathcal{M}_\ell}\|_1 \leq \|u_{\mathcal{M}_\ell}\|_1 + \|g_{\mathcal{M}_\ell}\|_1 < +\infty$. By the regularity of ψ we deduce

$$|Z_\ell| \leq h_{\mathcal{T}_\ell} \|\psi\|_\infty B_1 \|v_{\mathcal{M}_\ell}\|_1 \leq h_{\mathcal{T}_\ell} B_2 \xrightarrow[\ell \to +\infty]{} 0.$$

Now, developing the discrete gradient expression in Y_ℓ and making use of the discrete integration by parts lead to

$$\begin{aligned} Y_\ell = &-\frac{1}{2} \sum_{C \in \mathcal{T}_\ell} v_C \sum_{\mathbf{v} \in \mathcal{S}_C} d'_{C,\mathbf{v}} \psi_{\sigma_{C,\mathbf{v}}} \cdot \mathbf{n_{C,v}} \\ &-\frac{1}{2} \sum_{\mathbf{v} \in \mathcal{S}_\ell \backslash \mathcal{S}^D} v_{\mathbf{v}} \sum_{C \in \mathcal{T}_{\mathbf{v}}} \sum_{\nu \in \mathcal{S}_{C,\mathbf{v}}} d'_{C,\nu} \psi_{\sigma_{C,\nu}} \cdot \mathbf{n}_{C,\nu} \\ &-\frac{1}{2} \sum_{C \in \mathcal{T}_\ell} \sum_{\mathbf{v} \in \mathcal{S}_C} d_{C,\mathbf{v}} \big(v_{\sigma_{\mathbf{vv}'}} - v_{\sigma_{\mathbf{vv}^\star}}\big) \psi_{\sigma'_{C,\mathbf{v}}} \cdot \mathbf{n}'_{C,\mathbf{v}}, \end{aligned}$$

where we consider

$$v_{\sigma_{\mathbf{vv}'}} = \frac{1}{2}(v_{\mathbf{v}} + v_{\mathbf{v}'}), \quad v_{\sigma_{\mathbf{vv}^\star}} = \frac{1}{2}(v_{\mathbf{v}} + v_{\mathbf{v}^\star}).$$

Thanks to the divergence theorem we compute

$$\begin{aligned} &\sum_{C \in \mathcal{T}_\ell} v_C \sum_{\mathbf{v} \in \mathcal{S}_C} d'_{C,\mathbf{v}} \psi_{\sigma_{C,\mathbf{v}}} \cdot \mathbf{n_{C,v}} + \sum_{\mathbf{v} \in \mathcal{S}_\ell \backslash \mathcal{S}^D} v_{\mathbf{v}} \sum_{C \in \mathcal{T}_{\mathbf{v}}} \sum_{\nu \in \mathcal{S}_{C,\mathbf{v}}} d'_{C,\nu} \psi_{\sigma_{C,\nu}} \cdot \mathbf{n}_{C,\nu} \\ &= \sum_{C \in \mathcal{T}_\ell} v_C \int_{T_C} \nabla \cdot \psi \, \mathrm{d}x + \sum_{\mathbf{v} \in \mathcal{S}_\ell \backslash \mathcal{S}^D} v_{\mathbf{v}} \int_{T_{\mathbf{v}}} \nabla \cdot \psi \, \mathrm{d}x. \end{aligned}$$

It is useful to first specify some auxiliary notations. To this purpose, we denote by $\mathcal{E}_\ell$ the set of the mesh edges. Each edge $e_{\sigma_{\mathbf{vv}^\star}}$ is shared by two cells C and $C^\star$. The region $T_{\mathbf{vv}^\star}$ denotes the subdomain whose vertices are labeled by $C, \mathbf{v}, C^\star, \mathbf{v}^\star$. Then, similar computations as above imply

$$\begin{aligned} Y_\ell &= -\frac{1}{2} \int_\Omega v_{h_\ell} \nabla \cdot \psi \, \mathrm{d}x - \frac{1}{2} \sum_{e_{\sigma_{\mathbf{vv}^\star}} \in \mathcal{E}_\ell} v_{\sigma_{\mathbf{vv}^\star}} \sum_{\sigma'_{C,\mathbf{v}} \in \mathcal{E}_{\mathbf{vv}^\star}} d_{C,\mathbf{v}} \psi_{\sigma'_{C,\mathbf{v}}} \cdot \mathbf{n}'_{C,\mathbf{v}} \\ &= -\frac{1}{2} \int_\Omega v_{h_\ell} \nabla \cdot \psi \, \mathrm{d}x - \frac{1}{2} \sum_{e_{\sigma_{\mathbf{vv}^\star}} \in \mathcal{E}_\ell} v_{\sigma_{\mathbf{vv}^\star}} \int_{\partial T_{\mathbf{vv}^\star}} \psi \cdot \mathbf{n} \, \mathrm{d}s \\ &= -\frac{1}{2} \int_\Omega v_{h_\ell} \nabla \cdot \psi \, \mathrm{d}x - \frac{1}{2} \int_\Omega \widehat{v}_{h_\ell} \nabla \cdot \psi \, \mathrm{d}x, \end{aligned}$$

where $\widehat{v}_{h_\ell}$ designates the piecewise constant function which is equal to $v_{\sigma_{\mathbf{vv}^\star}}$ in $T_{\mathbf{vv}^\star}$ for each $e_{\sigma_{\mathbf{vv}^\star}}$. It remains to establish that

$$\lim_{\ell \to +\infty} A_\ell = \lim_{\ell \to +\infty} \frac{1}{2} \int_\Omega \big(v_{h_\ell} - \widehat{v}_{h_\ell}\big) \nabla \cdot \psi \, \mathrm{d}x = 0.$$

Indeed, it suffices to develop $\|v_{h_\ell} - \widehat{v}_{h_\ell}\|^2_{L^2(\Omega)}$ on the quarters of the diamond $|\mathcal{D}_{C,\mathbf{v}}|$ and estimate the result to find

$$\begin{aligned} \|v_{h_\ell} - \widehat{v}_{h_\ell}\|^2_{L^2(\Omega)} &\leq B_3 h^2_{\mathcal{T}_\ell} \sum_{C \in \mathcal{T}_\ell} \sum_{\mathbf{v} \in \mathcal{S}_C} \Big(|v_C - v_{\mathbf{v}}|^2 + |v_C - v_{\mathbf{v}'}|^2 + |v_C - v_{\mathbf{v}^\star}|^2 \Big) \\ &\leq B_4 h^2_{\mathcal{T}_\ell} \sum_{C \in \mathcal{T}_\ell} \sum_{\mathbf{v} \in \mathcal{S}_C} \Big(d^2_{C,\mathbf{v}} |\nabla_{\mathcal{D}_{C,\mathbf{v}}} v_{\mathcal{M}_\ell}|^2 + d^2_{C,\mathbf{v}'} |\nabla_{\mathcal{D}_{C,\mathbf{v}'}} v_{\mathcal{M}_\ell}|^2 + d^2_{C,\mathbf{v}^\star} |\nabla_{\mathcal{D}_{C,\mathbf{v}^\star}} v_{\mathcal{M}_\ell}|^2 \Big) \\ &\leq B_5 h^2_{\mathcal{T}_\ell} \sum_{C \in \mathcal{T}_\ell} \sum_{\mathbf{v} \in \mathcal{S}_C} \Big(|\mathcal{D}_{C,\mathbf{v}}| |\nabla_{\mathcal{D}_{C,\mathbf{v}}} v_{\mathcal{M}_\ell}|^2 + |\mathcal{D}_{C,\mathbf{v}'}| |\nabla_{\mathcal{D}_{C,\mathbf{v}'}} v_{\mathcal{M}_\ell}|^2 \\ &\qquad + |\mathcal{D}_{C,\mathbf{v}^\star}| |\nabla_{\mathcal{D}_{C,\mathbf{v}^\star}} v_{\mathcal{M}_\ell}|^2 \Big) \\ &\leq B_6 h^2_{\mathcal{T}_\ell} \xrightarrow[\ell \to +\infty]{} 0. \end{aligned}$$

As a consequence, one ends up with

$$\int_\Omega \mathbf{G}\cdot\psi\,\mathrm{d}x = -\int_\Omega v\nabla\cdot\psi\,\mathrm{d}x.$$

This proves that $\mathbf{G}=\nabla v$ a.e. in Ω and therefore $v\in H_0^1(\Omega)$. Accordingly, it follows from (3.13) that $u=v-g\in H^1(\Omega)$ and $\gamma(u)=\gamma(g)$. Next, the solution u should satisfy the weak formulation of (1.4). To this end, let $\varphi\in\mathcal{C}_c^\infty(\Omega)$ and consider $\varphi_{\mathcal{M}_\ell}$ the vector of $X_{\mathcal{M}_\ell,0}$ defined by

$$\varphi_K=\frac{1}{|K|}\int_K\varphi(x)\,\mathrm{d}x,\quad\forall K\in\mathcal{M}_\ell\setminus\mathcal{S}^D.$$

Passing to the limit in the discrete variational formulation (1.4) gives

$$\lim_{\ell\to+\infty}\int_\Omega\kappa_{h_\ell,\mathcal{T}_\ell}\nabla_{h_\ell}u_{h_\ell}\cdot\nabla_{h_\ell}\varphi_{h_\ell}\,\mathrm{d}x=\lim_{\ell\to+\infty}\int_\Omega f\varphi_{h_\ell}\,\mathrm{d}x=\int_\Omega f\varphi\,\mathrm{d}x.$$

Owing to (1.3a) together with (2.3), we have

$$\kappa_{h_\ell,\mathcal{T}_\ell}\xrightarrow[\ell\to+\infty]{}\kappa\quad\text{a.e. in }\Omega.$$

Additionally, the smoothness of φ and the Lebesgue dominated convergence theorem ensures then the strong convergence of $\kappa_{h_\ell,\mathcal{T}_\ell}\nabla_{h_\ell}\varphi_{h_\ell}$ towards $\kappa\nabla\varphi$. Whence, it is shown that

$$\int_\Omega\kappa\nabla u\cdot\nabla\varphi\,\mathrm{d}x=\int_\Omega f\varphi\,\mathrm{d}x,\quad\forall\varphi\in\mathcal{C}_c^\infty(\Omega).$$

Using a standard argument of density, this relationship is satisfied for all $\varphi\in H_0^1(\Omega)$.

Concerning the strong convergence of the approximate gradients, it is identical to the one elaborated in [20, Theorem 4.1]. We apply the same reasoning on $v_{\mathcal{M}_\ell}$ and thereby derive (3.15) by virtue of (3.13). This concludes the proof of Theorem 3.1. □

4 Numerical results

In this section, we implement and validate the developed numerical scheme (3.2)-(3.4). The objective is to show that the Node-Diamond method produces accurate results over various discretizations of the computational domain, and typical anisotropic and heterogeneous tensors.

For all the tests below, we consider the unit square domain $\Omega=(0,1)\times(0,1)$. It is meshed by 6 different successively refined meshes mostly taken from the FVCA benchmark [24] on the diffusion problems. They include structured, non-structured, conforming, non-conforming and distorted meshes. An illustration of them is depicted in Figure 2. For shortness, they will be referred to as **Tri**, **Quad**, **Kersh**, **LocRef**, **Cart**, **Diam**. This last one is built on a triangular mesh.

4.1 Implementation and resolution

Here, we survey the practical implementation of the Node-Diamond method and show that the stiffness matrix has a particular structure simplifying the resolution. This aspect is one of the main features of our scheme.

Given the mesh data, notably the cells and the vertices, the main connectivity list is a table **Vf** of 5 columns and $\sum_{C\in\mathcal{T}}\sum_{\mathbf{v}\in\mathcal{S}_C}\#\mathcal{S}_C$ lines. Independently of the chosen mesh, each line contains the information on the diamonds $\mathcal{D}_{C,\mathbf{v}}$ and it is made of $\big[C,\mathbf{v},\mathbf{v}',\mathbf{v}^\star\big]$.

All computations are carried out using this structure, in particular for normal vectors and length of interfaces. To identify the location of a given vertex $\mathbf{v}\in\mathcal{S}$, we use the local indicator $\mathbf{Id}_\mathbf{v}$ which is equal to 0 if $\mathbf{v}$ is a boundary vertex and to 1 if it is in the domain interior. We set $\overline{\mathbf{Id}}_\mathbf{v}=1-\mathbf{Id}_\mathbf{v}$.

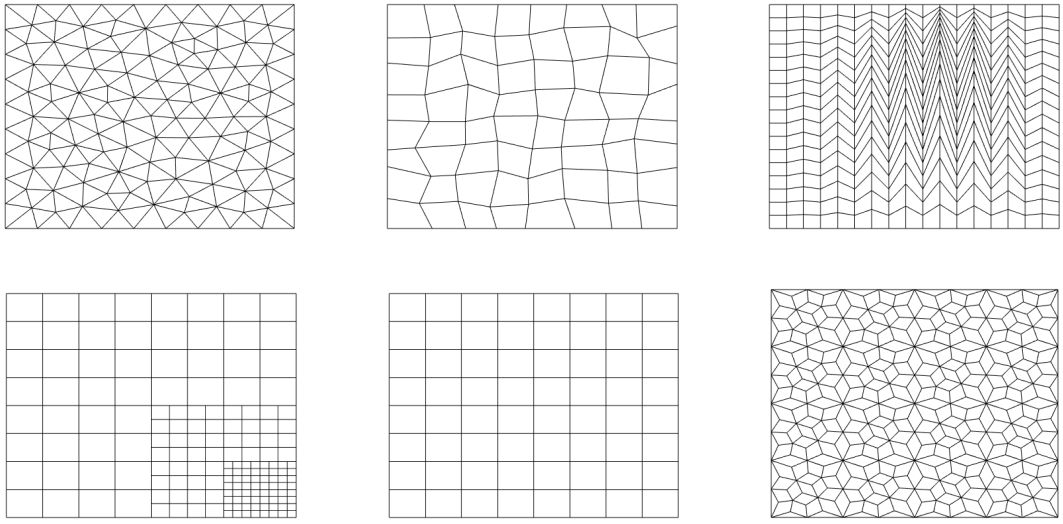

Figure 2: From left to right: Cartesian, triangular, random, locally refined, Kershaw, and diamond meshes.

The resolution of the Node-Diamond scheme (3.2)-(3.4) requires to rewrites its equations under the form of the linear system

$$\mathbf{A}u_{\mathcal{M}} = \mathbf{b}_{\mathcal{M}},$$

where $\mathbf{A}$ is a symmetric positive-definite matrix. The assembling of $\mathbf{A}$ is performed by adding the contribution of each diamond following the structure of **Vf**. First, the cell-vertex $(C \to \mathbf{v})$ and the vertex-vertex $(\mathbf{v}^\star \to \mathbf{v}')$ contributions stem from

$$\begin{aligned} F_{C,\mathbf{v}} &= \alpha_{C\mathbf{v}}(u_C - \mathbf{Id}_{\mathbf{v}}u_{\mathbf{v}}) + \beta_{C\mathbf{v}}(\mathbf{Id}_{\mathbf{v}^\star}u_{\mathbf{v}^\star} - \mathbf{Id}_{\mathbf{v}'}u_{\mathbf{v}'}),\\ F_{\mathbf{v}^\star,\mathbf{v}'} &= \alpha'_{\mathbf{v}C}(u_{\mathbf{v}^\star} - \mathbf{Id}_{\mathbf{v}'}u_{\mathbf{v}'}) + \beta_{C\mathbf{v}}(u_C - \mathbf{Id}_{\mathbf{v}}u_{\mathbf{v}}), \quad \mathbf{v}^\star \in \mathcal{S}_C \setminus \mathcal{S}^D, \end{aligned}$$

where

$$\alpha_{C\mathbf{v}} = \frac{1}{2\,|\mathcal{D}_{C,\mathbf{v}}|}(d'_{C,\mathbf{v}})^2\kappa_C\mathbf{n}_{\mathbf{C},\mathbf{v}}\cdot\mathbf{n}_{\mathbf{C},\mathbf{v}}, \quad \beta_{C\mathbf{v}} = \frac{1}{4\,|\mathcal{D}_{C,\mathbf{v}}|}d_{C,\mathbf{v}}d'_{C,\mathbf{v}}\kappa_C\mathbf{n}_{\mathbf{C},\mathbf{v}}\cdot\mathbf{n}'_{\mathbf{C},\mathbf{v}},$$
$$\alpha'_{C\mathbf{v}} = \frac{1}{8\,|\mathcal{D}_{C,\mathbf{v}}|}d^2_{C,\mathbf{v}}\kappa_C\mathbf{n}'_{\mathbf{C},\mathbf{v}}\cdot\mathbf{n}'_{\mathbf{C},\mathbf{v}}.$$

Second, observe that the contribution vertex-cell $(\mathbf{v} \to C)$ is filled owing to the symmetry i.e. using $F_{\mathbf{v},C} = -F_{C,\mathbf{v}}$ as long as $\mathbf{v} \notin \mathcal{S}^D$. A similar fact holds for $(\mathbf{v}' \to \mathbf{v}^\star)$. Additionally, the contribution of the boundary condition is assembled by considering

$$F_{\mathbf{v}^\star,\mathbf{v}^\star} = u_{\mathbf{v}^\star}, \quad \forall \mathbf{v}^\star \in \mathcal{S}^D.$$

Concerning the right hand side $\mathbf{b}_{\mathcal{M}} = (\mathbf{b}_{\mathcal{S}}, \mathbf{b}_{\mathcal{T}})^t$, it takes into account the non-homogeneous Dirichlet boundary condition as follows

$$\begin{aligned} b_C &= |T_C|\, f_{T_C} + \sum_{\mathbf{v}\in\mathcal{S}_C}\Big(\alpha_{C\mathbf{v}}\overline{\mathbf{Id}}_{\mathbf{v}}g_{\mathbf{v}} - \beta_{C\mathbf{v}}(\overline{\mathbf{Id}}_{\mathbf{v}^\star}g_{\mathbf{v}^\star} - \overline{\mathbf{Id}}_{\mathbf{v}'}g_{\mathbf{v}'})\Big),\\ b_{\mathbf{v}^\star} &= |T_{\mathbf{v}^\star}|\, f_{T_{\mathbf{v}^\star}} + \sum_{C\in\mathcal{T}_{\mathbf{v}^\star}}\Big(\alpha'_{\mathbf{v}C}\overline{\mathbf{Id}}_{\mathbf{v}'}g_{\mathbf{v}'} + \beta_{C\mathbf{v}}\overline{\mathbf{Id}}_{\mathbf{v}}g_{\mathbf{v}}\Big), \quad \mathbf{v}^\star \in \mathcal{S}_C \setminus \mathcal{S}^D,\\ b_{\mathbf{v}^\star} &= g_{\mathbf{v}^\star}, \quad \mathbf{v}^\star \in \mathcal{S}^D. \end{aligned}$$

The structure of the final stiffness matrix is composed of four blocks

$$\mathbf{A} = \begin{pmatrix} \mathbf{A}_{\mathcal{S}} & \mathbf{A}_{\mathcal{S},\mathcal{T}} \\ \mathbf{A}_{\mathcal{T},\mathcal{S}} & \mathbf{A}_{\mathcal{T}} \end{pmatrix}.$$

The size of each block is given by : size($\mathbf{A}_{\mathcal{S}}$) = $\#\mathcal{S} \times \#\mathcal{S}$, size($\mathbf{A}_{\mathcal{T},\mathcal{S}}$) = $\#\mathcal{T} \times \#\mathcal{S}$, size($\mathbf{A}_{\mathcal{S},\mathcal{T}}$) = $\#\mathcal{S} \times \#\mathcal{T}$, size($\mathbf{A}_{\mathcal{T}}$) = $\#\mathcal{T} \times \#\mathcal{T}$. The block $\mathbf{A}_{\mathcal{T}}$ is an invertible diagonal matrix. Then, the structure of $\mathbf{A}$ is more appealing since the Schur complement can be calculated in a straightforward way. As a consequence, the cell unknowns are eliminated before the resolution process. The resolution task amounts to solving the reduced linear system involving only vertex unknowns

$$\big(\mathbf{A}_{\mathcal{S}} - \mathbf{A}_{\mathcal{S},\mathcal{T}}\mathbf{A}_{\mathcal{T}}^{-1}\mathbf{A}_{\mathcal{T},\mathcal{S}}\big)u_{\mathcal{S}} = \mathbf{b}_{\mathcal{S}} - \mathbf{A}_{\mathcal{S},\mathcal{T}}\mathbf{A}_{\mathcal{T}}^{-1}\mathbf{b}_{\mathcal{T}}.$$

Finally, this allows to easily compute cell unknowns using the relationship

$$u_{\mathcal{T}} = \mathbf{A}_{C}^{-1}\big(\mathbf{b}_{\mathcal{T}} - \mathbf{A}_{C,\mathbf{v}}u_{\mathcal{S}}\big).$$

We are interested in evaluating the errors between the exact and numerical solutions in the sense of the L^2-norm and H^1-norm respectively given by

$$E_{L^2} := \left(\sum_{C\in\mathcal{T}} |T_C|\,|u_e(x_C) - u_C|^2 + \sum_{\mathbf{v}\in\mathcal{S}} |T_{\mathbf{v}}|\,|u_e(x_{\mathbf{v}}) - u_{\mathbf{v}}|^2\right)^{1/2},$$

$$E_{H^1} := \left((E_{L^2})^2 + \sum_{C\in\mathcal{T}}\sum_{\mathbf{v}\in\mathcal{S}_C} |\mathcal{D}_{C,\mathbf{v}}|\,\big|\nabla u_e(x_{C,\mathbf{v}}) - \nabla_{\mathcal{D}_{C,\mathbf{v}}} u_{\mathcal{M}}\big|^2\right)^{1/2},$$

where $x_{C,\mathbf{v}}$ denotes the mass center of $\mathcal{D}_{C,\mathbf{v}}$.

4.2 Test 1 : homogeneous problem

In this first numerical example, we test the Node-Diamond scheme with no impact of the diffusion tensor. We consider the function

$$u_e(x) = \cos(0.5\pi x_1), \quad x = (x_1, x_2) \in \Omega,$$

as an exact solution to Poisson's equation. The source term and the imposed Dirichlet boundary condition correspond to this solution. The tensor κ is homogeneous i.e. $\kappa = Id$, where Id refers to the identity matrix. The obtained numerical errors are depicted in Figure 3 using the log-log scale. A quadratic convergence is observed with respect to the L^2-norm while a linear convergence of first order is noticed in terms of the H^1-norm. Therefore, the proposed numerical scheme yields similar optimal rates as in the literature independently of the selected mesh.

	Tri	**Quad**	**Kersh**	**LocRef**	**Cart**	**Diam**
$u_{\min}$	0.0000	0.0000	0.0000	0.0000	0.0000	0.0000
$u_{\max}$	1.0049	1.0006	1.0000	1.0000	1.0000	1.0024

Table 1: Test 1: DMP on the first element for each category of meshes.

We also evaluate the discrete maximum principle (DMP) in Table 1 on the coarsest elements of the considered meshes. For this test-case, the approximate solution has no undershoots, but small overshoots are noticed on some meshes, namely **Tri**, **Quad** and **Diam**. According to Remark 3.1 the stiffness matrix enjoys the M-matrix structure in the case of Cartesian meshes made of squares. As a result, the Node-Diamond scheme is necessary monotone. This fact is clearly seen Table 1.

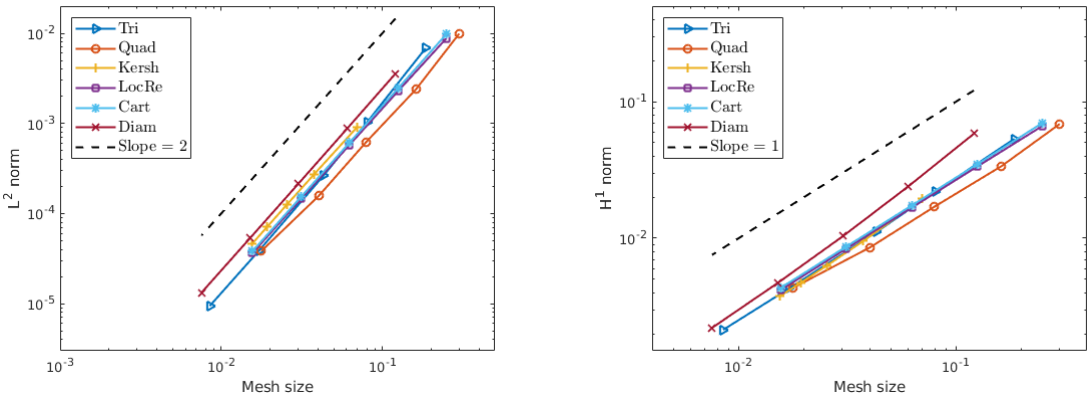

Figure 3: Test 1: numerical errors in the discrete L^2-norm (left) and H^1-norm (right) with a homogeneous isotropic diffusion.

4.3 Test 2 : strongly anisotropic example

In this numerical test, we focus on the robustness and accuracy of the proposed scheme in the case of a strong anisotropic diffusion matrix. The latter is defined by

$$\kappa(x) = \begin{pmatrix} 1 & 0 \\ 0 & 100 \end{pmatrix}.$$

We consider the following exact solution to the elliptic model (1.1)-(1.2)

$$u_e(x) = 16x_1(1-x_1)x_2(1-x_2), \quad x = (x_1, x_2) \in \Omega,$$

where the source term is computed using this solution. Homogeneous Dirichlet boundary conditions are taken into account. The obtained numerical convergence of the scheme is exhibited in Figure 4. As in the first test, second order accuracy is obtained for the L^2-errors and a linear rate is still maintained for the H^1-errors regardless anisotropy.

The discrete maximum principle is summed up in Table 2. The lower bound is well honored whereas the upper one exceeds the corresponding analytical value on almost all meshes, which is due to the mesh nature and the anisotropy effect. This is a standard fact in the approximation of the anisotropic elliptic equations on general meshes [24].

	Tri	**Quad**	**Kersh**	**LocRef**	**Cart**	**Diam**
$u_{\min}$	0.0000	0.0000	0.0000	0.0000	0.0000	0.0000
$u_{\max}$	1.0906	1.2026	1.0404	1.1220	1.0592	0.9867

Table 2: Test 2: DMP on the first element of each mesh category.

4.4 Test 3 : case of heterogeneous rotating anisotropy

In this section, we perform a numerical test using the proposed scheme in the case of anisotropic and heterogeneous tensor. In the discrete level, the tensor is considered constant per cell. We consider the following example used in [17] where the analytical solution is as follows

$$u_e(x) = \sin(\pi x_1)\sin(\pi x_2), \quad x = (x_1, x_2) \in \Omega.$$

As previously, the boundary condition agrees with the trace function of u_e. The source term is determined from the solution and the following space-dependent tensor

$$\kappa(x) = \begin{pmatrix} \varepsilon\widehat{x}_1^2 + \widehat{x}_2^2 & -(1-\varepsilon)\widehat{x}_1\widehat{x}_2 \\ -(1-\varepsilon)\widehat{x}_1\widehat{x}_2 & \widehat{x}_1^2 + \varepsilon\widehat{x}_2^2 \end{pmatrix},$$

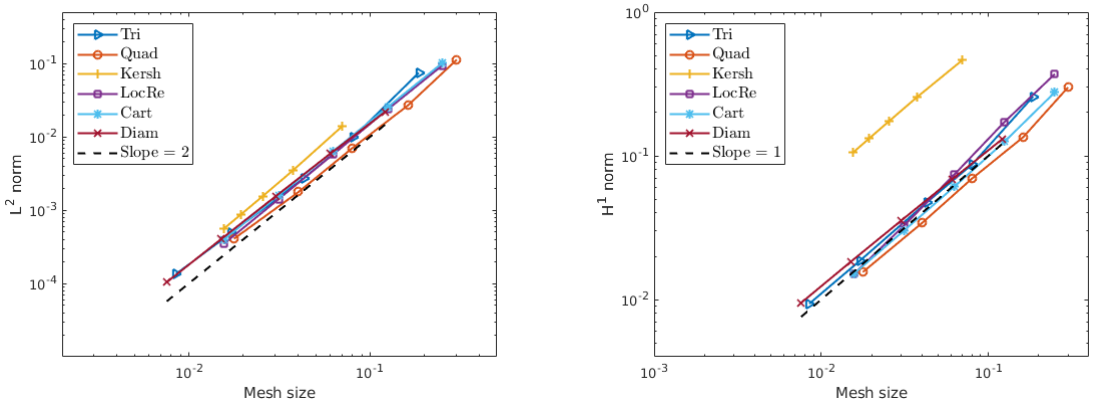

Figure 4: Test 2: numerical errors in the discrete L^2-norm (left) and H^1-norm (right) with a weakly homogeneous anisotropic diffusion.

where we set $\widehat{x}_1 = x_1 - 0.1$ and $\widehat{x}_2 = x_2 - 0.1$. The parameter ε is equal to 10^{-4}. The accuracy results are shown in Figure 5. It is noticed that the obtained convergence rates are not influenced neither by the anisotropy ratio together with the heterogeneity of κ nor the considered mesh, which confirms the robustness of this novel approach. According to Table 3, undershoots are reported besides to the overshoots.

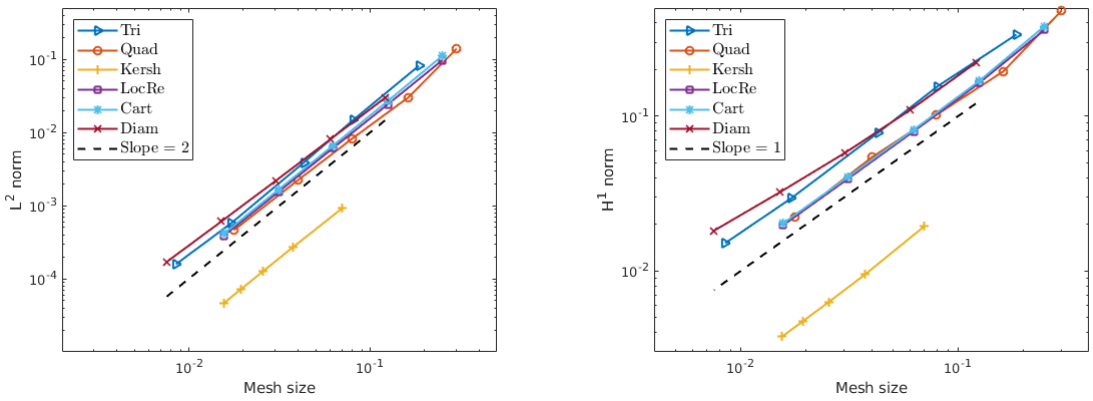

Figure 5: Test 3: numerical errors in the discrete L^2-norm (left) and H^1-norm (right) with a heterogeneous rotating anisotropic diffusion.

	Tri	**Quad**	**Kersh**	**LocRef**	**Cart**	**Diam**
$u_{\min}$	-0.0203	0.0000	0.0000	0.0000	0.0000	-0.0390
$u_{\max}$	1.0773	1.1302	1.1173	1.1395	1.0592	0.9988

Table 3: Test 3: DMP on the first element of each mesh category.

4.5 Test 4 : domain with a vertical fault

We look at a relevant test-case of the FVCA5 benchmark refereed to as "Vertical Fault". The meshed domain includes a crossed fault. This gives rise to nonconforming staggered grids. An illustration of that is given in the left subfigure of Figure 6. The white region is denoted by Ω_w

and the colored part is denoted by $\Omega_c := \Omega \setminus \overline{\Omega}_w$. The cells of each subdomain are rectangular. We consider a highly anisotropic situation with

$$\kappa_{|\Omega_w}(x) = \begin{pmatrix} 0.01 & 0 \\ 0 & 0.001 \end{pmatrix}, \quad \text{and} \quad \kappa_{|\Omega_c}(x) = \begin{pmatrix} 1000 & 0 \\ 0 & 100 \end{pmatrix}.$$

The source term is fixed to $f = 0$. The diffusion process is governed by κ and the Dirichlet boundary condition

$$u_e(x) = 1 - x_1, \quad (x_1, x_2) \in \partial\Omega.$$

The produced numerical solution is plotted on the right hand side of Figure 6. The effects of anisotropy together with the fault impact are well captured by our scheme even though the mesh is coarse. The solution is similar to the one provided in [24]. Furthermore, the discrete maximum principle is respected.

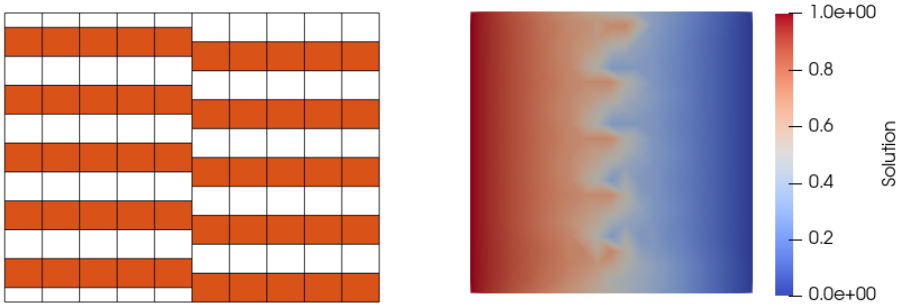

Figure 6: Staggered mesh (left), the anisotropy is defined by colored region, as well as the numerical solution (right).

4.6 Test 5 : oblique flow

In this last example, we explore the behavior of the proposed Node-Diamond scheme using another challenging test-case taken from the FVCA5 benchmark with the same set up. It is termed as the oblique flow. The diffusion tensor is defined as follows

$$\kappa(x) = \mathcal{R}(\theta) \times \begin{pmatrix} 1 & 0 \\ 0 & 0.001 \end{pmatrix} \times \mathcal{R}^{-1}(\theta), \quad \text{and} \quad \mathcal{R}(\theta) = \begin{pmatrix} \cos(\theta) & -\sin(\theta) \\ \sin(\theta) & \cos(\theta) \end{pmatrix},$$

where the rotation angle is $\theta = 40$ degrees. The source function f is set to 0. The Dirichlet boundary condition is prescribed by the piecewise continuous function

$$u_e(x) = \begin{cases} 1 & \text{on } (0, 0.2) \times \{0\} \bigcup \{0\} \times (0, 0.2) \\ 0 & \text{on } (0.8, 1) \times \{1\} \bigcup \{1\} \times (0.8, 1) \\ 0.5 & \text{on } (0.3, 1) \times \{0\} \bigcup \{0\} \times (0.3, 1) \\ 0.5 & \text{on } (0, 0.7) \times \{1\} \bigcup \{1\} \times (0, 0.7) \end{cases}.$$

We run the scheme algorithm on the first three Cartesian meshes with the aforementioned inputs. The results are displayed on Figure 7. The solution form is visibly identified on the coarsest mesh (4×4) cells and takes a clearer shape as the mesh is refined. Small undershoots are noted as the color bar shows.

5 Conclusion and perspectives

We proposed a nodal numerical scheme for the approximation of heterogeneous and anisotropic elliptic equations over quite general polygonal meshes. Our approach consists in designing discrete gradients, over local embedded diamonds per cells, that are injected in a discrete weak

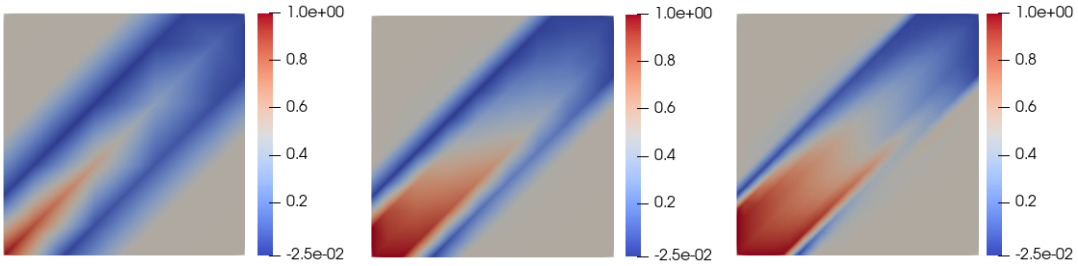

Figure 7: From left to right : approximate solution of the oblique flow test-case on three Cartesian meshes ($\mathbf{Cart}_1$, $\mathbf{Cart}_2$ and $\mathbf{Cart}_3$).

formulation to obtain the Node-Diamond scheme. The objective is to unconditionally inherit at the discrete level some structural properties such as the discrete Poincaré's inequality and the coercivity. We surveyed a natural extension to the case of additional advection by means of classical finite volume techniques. By proving an asymptotic Stokes' formula, the scheme is shown to converge under general assumptions on the physical parameters of the model equation and the mesh. We stress that the cell equation is made of cell-vertex contributions involving only d.o.f connected to the vertex in question. As a result, the computational cost is improved by eliminating the cell unknowns thanks to a simple static condensation. A practical implementation of the Node-Diamond approach can be carried out using only the cell-vertex connectivity. Numerical results exhibited and validated the excellent behavior of the method.

As a first perspective, we wish to extend these ideas of the Node-Diamond methodology to three dimensions so that a broad range of realistic and industrial applications can be covered. Second, it will be interesting to develop and examine a version of the scheme in case of coupled degenerate nonlinear parabolic equations motivated by applications in systems of population dynamics and chemotaxis. Third, we intend to investigate its generalization to complex flows in heterogeneous porous media with more stability quests like the satisfaction of the discrete maximum principle.

Acknowledgment: the first author would like to thank the Département de la Marne, Greater Reims, Région Grand Est for their financial support of the Chair of Biotechnology of CentraleSupélec.

References

[1] I. Aavatsmark. An introduction to multipoint flux approximations for quadrilateral grids. *Computational Geosciences*, 6(3):405–432, 2002.

[2] I. Aavatsmark, T. Barkve, O. Bøe, and T. Mannseth. Discretization on unstructured grids for inhomogeneous, anisotropic media. Part I: Derivation of the methods. *SIAM Journal on Scientific Computing*, 19(5):1700–1716, 1998.

[3] I. Aavatsmark, T. Barkve, O. Bøe, and T. Mannseth. Discretization on unstructured grids for inhomogeneous, anisotropic media. Part II: Discussion and numerical results. *SIAM Journal on Scientific Computing*, 19(5):1717–1736, 1998.

[4] I. Aavatsmark, G. Eigestad, R. Klausen, M. Wheeler, and I. Yotov. Convergence of a symmetric MPFA method on quadrilateral grids. *Computational Geosciences*, 11(4):333–345, 2007.

[5] M. Afif and B. Amaziane. Convergence of finite volume schemes for a degenerate convection–diffusion equation arising in flow in porous media. *Computer Methods in Applied Mechanics and Engineering*, 191(46):5265–5286, 2002.

[6] B. Andreianov, F. Boyer, and F. Hubert. Discrete duality finite volume schemes for Leray–Lions–type elliptic problems on general 2D meshes. *Numerical Methods for Partial Differential Equations*, 23(1):145–195, 2007.

[7] F. Boyer and F. Hubert. Finite volume method for 2D linear and nonlinear elliptic problems with discontinuities. *SIAM Journal on Numerical Analysis*, 46(6):3032–3070, 2008.

[8] K. Brenner and R. Masson. Convergence of a vertex centred discretization of two-phase Darcy flows on general meshes. *International Journal on Finite Volumes*, 10:1–37, 2013.

[9] K. Brenner, R. Masson, and E. H. Quenjel. Vertex Approximate Gradient Discretization preserving positivity for two-phase Darcy flows in heterogeneous porous media. *Journal of Computational Physics*, 409:109357, 2020.

[10] F. Brezzi, K. Lipnikov, and V. Simoncini. A family of mimetic finite difference methods on polygonal and polyhedral meshes. *Mathematical Models and Methods in Applied Sciences*, 15(10):1533–1551, 2005.

[11] P. G. Ciarlet. *The finite element method for elliptic problems*. SIAM, 2002.

[12] B. Da Veiga, J. Droniou, and G. Manzini. A unified approach for handling convection terms in finite volumes and mimetic discretization methods for elliptic problems. *IMA Journal of Numerical Analysis*, 31(4):1357–1401, 2011.

[13] L. B. da Veiga, K. Lipnikov, and G. Manzini. *The mimetic finite difference method for elliptic problems*, volume 11. Springer, 2014.

[14] K. Domelevo and P. Omnes. A finite volume method for the Laplace equation on almost arbitrary two-dimensional grids. *ESAIM: Mathematical Modelling and Numerical Analysis*, 39(6):1203–1249, 2005.

[15] J. Droniou. Finite volume schemes for diffusion equations: introduction to and review of modern methods. *Mathematical Models and Methods in Applied Sciences*, 24(08):1575–1619, 2014.

[16] J. Droniou and R. Eymard. A mixed finite volume scheme for anisotropic diffusion problems on any grid. *Numerische Mathematik*, 105(1):35–71, 2006.

[17] J. Droniou, R. Eymard, T. Gallouët, C. Guichard, and R. Herbin. *The gradient discretisation method*, volume 82. Springer, 2018.

[18] J. Droniou, R. Eymard, T. Gallouët, and R. Herbin. A unified approach to mimetic finite difference, hybrid finite volume and mixed finite volume methods. *Mathematical Models and Methods in Applied Sciences*, 20(02):265–295, 2010.

[19] R. Eymard, T. Gallouët, and R. Herbin. Finite volume methods. In *Handbook of Numerical Analysis*, volume 7, pages 713–1018. Elsevier, 2000.

[20] R. Eymard, T. Gallouët, and R. Herbin. Discretization of heterogeneous and anisotropic diffusion problems on general nonconforming meshes SUSHI: a scheme using stabilization and hybrid interfaces. *IMA Journal of Numerical Analysis*, 30(4):1009–1043, 2010.

[21] R. Eymard, C. Guichard, and R. Herbin. Small-stencil 3D schemes for diffusive flows in porous media. *ESAIM: Mathematical Modelling and Numerical Analysis*, 46(2):265–290, 2012.

[22] R. Eymard, D. Hilhorst, and M. Vohralík. A combined finite volume–nonconforming/mixed-hybrid finite element scheme for degenerate parabolic problems. *Numerische Mathematik*, 105(1):73–131, 2006.

[23] M. Ghilani, E. H. Quenjel, and M. Saad. Positive control volume finite element scheme for a degenerate compressible two-phase flow in anisotropic porous media. *Computational Geosciences*, 23(1):55–79, 2019.

[24] R. Herbin and F. Hubert. Benchmark on discretization schemes for anisotropic diffusion problems on general grids. In R. Eymard and J.-M. Herard, editors, *Finite Volumes for Complex Applications V*, pages 659–692. Wiley, 2008.

[25] F. Hermeline. A finite volume method for the approximation of diffusion operators on distorted meshes. *Journal of computational Physics*, 160(2):481–499, 2000.

[26] M. Ibrahim, E. H. Quenjel, and M. Saad. Positive nonlinear DDFV scheme for a degenerate parabolic system describing chemotaxis. *Computers & Mathematics with Applications*, 80(12):2972–3003, 2020.

[27] M. Ibrahim and M. Saad. On the efficacy of a control volume finite element method for the capture of patterns for a volume-filling chemotaxis model. *Computers & Mathematics with Applications*, 68(9):1032–1051, 2014.

[28] H. Karjoun, A. Beljadid, and P. G. LeFloch. A structure-preserving algorithm for surface water flows with transport processes. *Advances in Computational Mathematics*, under review, 2021.

[29] E. H. Quenjel. Nonlinear finite volume discretization for transient diffusion problems on general meshes. *Applied Numerical Mathematics*, 161:148–168, 2021.

[30] E. H. Quenjel. Positive Scharfetter-Gummel finite volume method for convection-diffusion equations on polygonal meshes. *Preprint*, 2021.

[31] D. L. Scharfetter and H. K. Gummel. Large-signal analysis of a silicon read diode oscillator. *IEEE Transactions on electron devices*, 16(1):64–77, 1969.